Sensitivity Analysis on Seismic Performance of Pile-Group Supported Bridges under Combined Effects of Scour and Liquefaction Hazards

Xiaowei Wang, Aff.M.ASCE[1]; and Aijun Ye[2]

[1]Assistant Professor, Dept. of Civil Engineering, Hohai Univ., 1 Xikang Rd., Nanjing 210024, China. E-mail: x.wang@hhu.edu.cn
[2]Professor, State Key Laboratory of Disaster Reduction in Civil Engineering, Tongji Univ., 1239 Siping Rd., Shanghai 200092, China. E-mail: yeaijun@tongji.edu.cn

ABSTRACT

Characterizing the effect of varying design parameters on the seismic performance of bridges can assist in optimum seismic design, especially for those in complex geotechnical conditions where scour and liquefaction hazards occur. This paper presents results of sensitivity analyses on the seismic performance of pile-group-supported bridges under combined effects of scour and liquefaction hazards. A fragility-based tornado diagram method is proposed for the sensitivity analyses. The studied parameters include the column height, diameter and axial compressive ratio, pile diameter and center-to-center distance, and relative densities of loose and dense sands. Special attentions are paid to the influence of scour depth on the sensitivity-ranking of the parameters. Main findings are that the pile diameter and center-to-center distance show increasing sensitivity with the increase of scour depth. These two parameters should be treated carefully in the seismic design of scoured bridges in liquefaction ground. On the contrary, relative densities of loose and dense sands that show significant influences for the scenario without scour turn to be the least sensitive parameters for scoured scenarios.

INTRODUCTION

Scour is reported to be one of the most severe hazards causing river-cross bridge failures in the United States (Deng et al. 2016). **Fig. 1** shows a typical river-cross multi-span bridge that was subjected to scour hazard. The upper portion of the pile-group foundation was exposed without surrounding soils due to scour. Meanwhile, saturated sands in scoured bridge sites may liquefy under strong earthquakes. Soil liquefaction-induced damage to piles and associated failure of bridges have been witnessed in several historical earthquakes (e.g. Bhattacharya et al. 2014). Previous studies, regardless of experiments or numerical analyses, on the seismic performance of bridges always considered the effect of liquefaction or scour separately (e.g., Brandenberg et al. 2005 and Wang et al. 2015, 2016b, among others). However, in practice, it tends to be a common scenario that bridges are located in flood-induced scour sites where the saturated sands may liquefy under earthquakes. The prediction of seismic performance of bridges in such complex geotechnical conditions requires special attentions for both the engineers and academic scholars.

Numerical predictions on the seismic performance of soil-bridge systems may be susceptible to varied design parameters. From a predictive point of view, it is desirable to characterize impacts of these parameters, which can assist in optimum seismic design of bridges. Using parametric or sensitivity analyses, previous studies mainly quantify these impacts on the seismic response or performance of bridges in scour or liquefiable conditions, separately (Brandenberg et al. 2008; Klinga and Alipour 2015; Padgett et al. 2010; Wang et al. 2016a). To the best knowledge of the authors, sensitivity analyses on the seismic performance of bridges under

combined effects of scour and liquefaction hazards are not well documented, let alone the impact of scour depth on sensitivities of the design parameters. These issues provide the motivation for the present study.

Fig. 1 Scour-induced exposure of pile foundations (By courtesy of Professor Yi-Ching Lin)

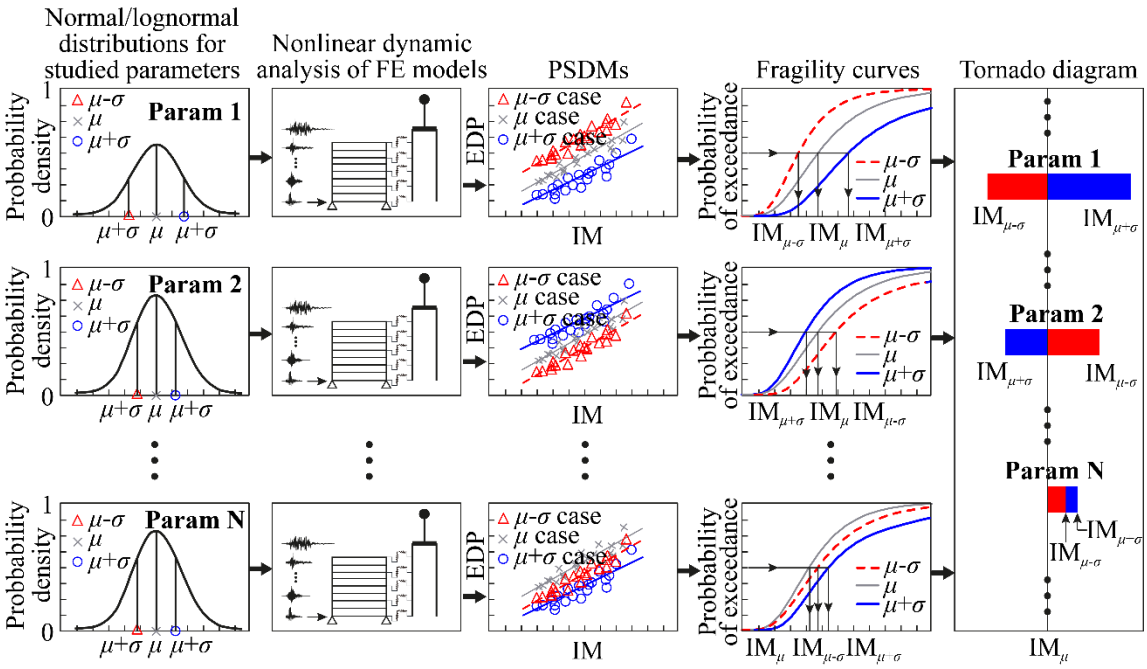

Fig. 2 Illustration of the fragility-based Tornado diagram for sensitivity analysis

This study performs sensitivity analyses to identify bridge design parameters that have the most and least significant effects on the seismic performance of bridges under combined effects of scour and liquefaction hazards. A fragility-based Tornado diagram method for the sensitivity analyses is introduced first. Then, coupled soil-bridge finite element (FE) models are built, which represent typical multi-span reinforced concrete bridges supported by pile-group foundations in scoured ground that may undergo liquefaction under earthquakes. Real site unscaled ground motions are selected for probabilistic seismic demand analyses, which are used to generate fragility curves. Finally, sensitivity results are discussed to provide insights into the seismic design of bridges under combined effects of scour and liquefaction.

PROPOSED METHOD FOR SENSITIVITY ANALYSES

There are several techniques for sensitivity analyses, mainly including Tornado diagram, First-Order Second-Moment and Monte Carlo simulation. Among them, the Monte Carlo simulation often requires heavy computational efforts, especially for this study where complex soil-foundation-structure interactions are involved for the nonlinear dynamic analyses. By comparison, Tornado diagram is an efficient solution from a view of practice. On the other hand, this study concentrates on the seismic performance assessment, rather than the seismic response merely. Hence, fragility analyses are used to rigorously estimate the seismic performance of bridges. In addition, fragility analyses can efficiently reveal the performance at multi-level damage states. Considering these merits, a fragility-based Tornado diagram method is proposed in the present study for the sensitivity analyses. **Fig. 2** illustrates the main process of this method, which is further described as follows.

For a parameter supposing a normal or lognormal distribution, two extreme values at 16th and 84th percentiles (i.e. mean, μ, minus and plus standard deviation, σ) are adopted as lower and upper bounds, respectively. A set of ground motions (described later) is used for dynamic analyses of three FE models where parameters with the lower, mean and upper values are involved, respectively. Probabilistic seismic demand analyses are performed to establish the corresponding three probabilistic seismic demand models (PSDMs). Accordingly, based on mathematical basis for fragility curves (Cornell et al. 2002), as well as the established PSDMs and pre-defined probabilistic capacity models, three fragility curves that reflect the impact of this parameter on the seismic performance of the bridges are generated using **Eq. (1)**.

$$P\left[D \geq C \mid IM\right] = 1 - \Phi\left(\frac{\ln\left(S_C\right) - \ln\left(S_D\right)}{\sqrt{\beta_C^2 + \beta_D^2}}\right) \tag{1}$$

where $\Phi(\bullet)$ is the standard normal cumulative distribution function, D is the demand, C is the capacity, S_D and S_C are median values of the demand and capacity, respectively, β_D and β_C are logarithmic standard deviations of the demand and capacity, respectively. Based on the fragility curves, intensity measure values at a given level of probability of exceedance (e.g., P_r = 50%, the so-called median fragility values) are obtained as "performance indices" (i.e., $IM_{\mu-\sigma}$, IM_{μ} and $IM_{\mu+\sigma}$, as shown in **Fig. 2**) for this parameter in the Tornado diagram. Note that blue bars in the Tornado diagram indicate $IM_{\mu+\sigma}$ while red bars represent $IM_{\mu-\sigma}$. Bars in the right side of the Tornado diagram represent cases with lower P_r. Repeating the above process for every studied design parameter. The obtained performance indices are sorted based on their ranges (from high to low) to fulfill the Tornado diagram. It is worth noting that for some parameters, the fragility curve derived from the model with the mean value (μ) may not lays between the upper ($\mu+\sigma$) and lower ($\mu-\sigma$) values-based fragility curves (see "Param N" in **Fig. 2**, in which part of the blue bar is covered by the red bar). In this regard, to consider the potential large distances between $IM_{\mu-\sigma}$ (or $IM_{\mu+\sigma}$) and IM_{μ} for such parameters, the abovementioned "ranges of performance indices" are defined using **Eq. (2)**:

$$\text{Ranges of performance indices} = \left|\text{IM}_{\mu+\sigma} - \text{IM}_{\mu}\right| + \left|\text{IM}_{\mu} - \text{IM}_{\mu-\sigma}\right| \tag{2}$$

where $|\bullet|$ is the absolute value operator.

NUMERICAL MODELS

A coupled multi-scale soil-bridge FE model is built in the *OpenSees* platform (McKenna 2011). **Fig. 3** shows the schematic illustration of the FE model. A two-dimensional plain-strain

soil model is linked to a three-dimensional simplified pile-group-supported bridge model using the Winkler-foundation-based *p-y*, *t-z* and *q-z* springs. This simplified multi-scale modelling technique has been validated by the authors (Wang et al. 2017) using three centrifuge tests in literature. Elastic rubber bearings (ERBs) are used to connect the single column with the lumped mass that represents the superstructure. It should be noted that this FE model represents typical multi-span reinforced concrete highway bridges or viaducts supported by multiple individual bents that have a fairly uniform distribution of strength and stiffness among them in the transverse direction (i.e., similar to the scenario shown in **Fig. 1**). For this reason, abutments are not considered in this study. More specifically, each bent consists of a single column supported by a commonly used 3×2 pile-group foundation embedded into saturated sands (loose sand overlying dense sand) that may undergo scour and earthquake-induced liquefaction hazards.

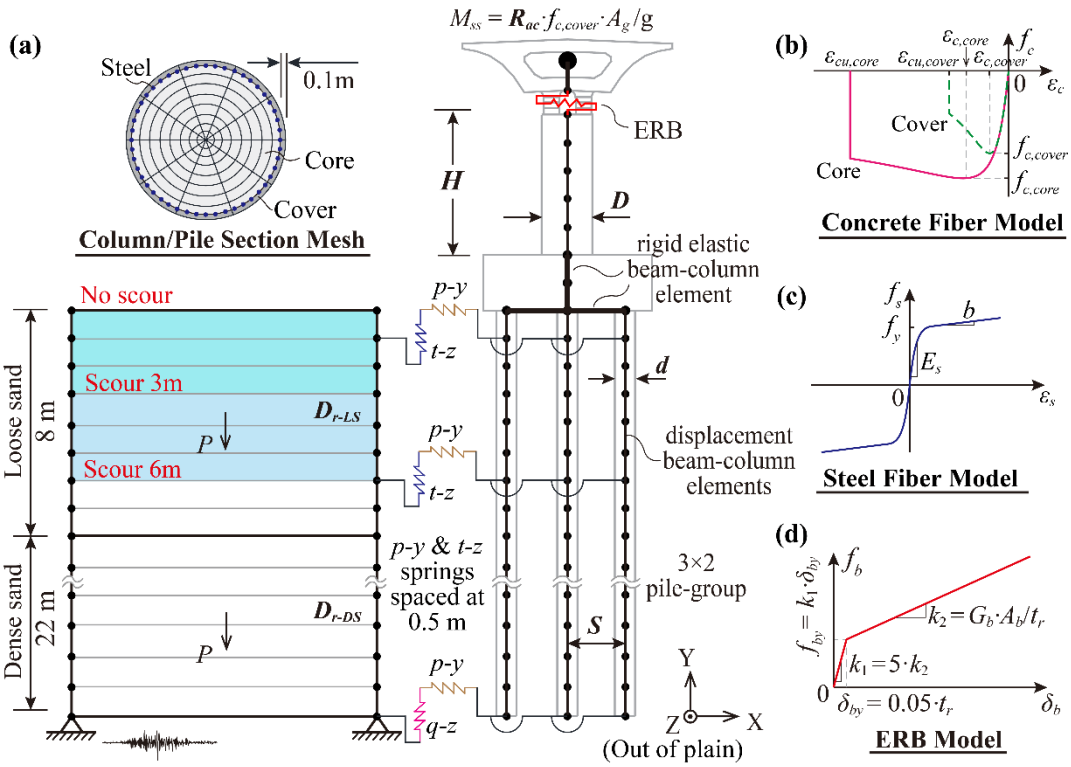

Fig. 3 FE model: (a) coupled bridge-soil-foundation model and section mesh, (b) concrete fiber model, (c) steel fiber model and (d) elastic rubber bearing model.

To assess the impact of scour depth on the sensitivity of seismic performance to design parameters, three scenarios in terms of scour depth are considered, including 0 m ("no scour", i.e., without scour), 3 m and 6 m (**Fig. 3(a)**), which generally cover the expected scour depths for the studied bridges. **Table 1** lists the studied seven parameters that are assumed to follow normal distributions, which are categized into column-, pile- and soil-related. Means and coefficient of variances (COVs) of the parameters are also listed, together with their upper and lower bounds for the sensitivity analyses. It is worth noting that the column axial compressive ratio (R_{ac}) is defined using **Eq. (3)**.

$$R_{ac} = \frac{M_{ss} \cdot g}{f_{c,cover} \cdot A_g} \tag{3}$$

where M_{ss} is superstructure mass supported by the column, g is the gravity constant, $f_{c,cover}$ is the

peak strength of concrete cover, and A_g is the gross area of the section. It should be noted that since information about COV values for R_{ac}, D, d and S (see **Table 1**) are not available in literature, they are determined based on in-depth communications with experienced bridge engineers, which roughly represent one standard derivation above and below the mean values. In total, one case with the mean values and fourteen cases with the lower and upper bounds (seven for each) are set up.

Table 1. Studied design parameters and their normal distribution properties

Parameters	Notation (Unit)	Mean	COV	Lower	Upper
Column-related					
Height	H (m)	6.5	0.26 [a]	4.8	8.2
Diameter	D (m)	2	0.10 [b]	1.8	2.2
Axial compressive ratio	R_{ac}	10%	0.20 [b]	8%	12%
Pile-related					
Diameter	d (m)	1	0.10 [b]	0.09	0.11
Center-to-center distance	S (m)	3d	0.15 [b]	2.5d	3.5d
Soil-related					
Loose sand relative density	$D_{r\text{-}LS}$	0.37	0.19 [c]	0.30	0.44
Dense sand relative density	$D_{r\text{-}DS}$	0.75	0.19 [c]	0.61	0.89

[a](Brandenberg et al. 2011);
[b]Assumed based on experienced engineering judgements;
[c](Jones et al. 2002).

The PDMY constitutive model in the *OpenSees* material library (McKenna 2011) is used to model the saturated sands (e.g., 8 m-thickness of loose sand overlying 22 m-thickness of dense sand for the "no scour" scenario). This soil model is assigned to the four-node QuadUP element that can simulate the behavior of solid-fluid coupled materials under cyclic excitation. The soil elements are meshed into 0.5 m along the depth, whereas the horizontal dimension and the out-of-plain thickness are assigned large values to assure a free-filed circumstance. *p-y* and *t-z* springs are spaced at 0.5 m consistent with the mesh of the soil elements. Pile-tips are linked to the soil elements using *q-z* springs. It is worth noting that model input variables for the PDMY material and QuadUP element as well as the soil springs can be determined based on $D_{r\text{-}LS}$ and $D_{r\text{-}DS}$, as listed in **Table 1**. For conciseness, more details can be found in Wang et al. (2017). In addition, to account for group effects for closely spaced piles, group efficiency factors of 0.7, 0.8 and 0.9 are selected for pile center-to-center distance, S = 2.5d, 3d and 3.5d, respectively (Mokwa 1999).

The 3×2 piles and single column are modeled using displacement-based beam-column elements (with fine meshed fiber sections) discretized into 0.5 m in depth. Each element adopts five integration points to achieve stable curvature responses. The concrete fibers are assigned using the Concrete04 material (**Fig. 2(b)**), while the steel fibers are modeled using the Steel02 material (**Fig. 2(c)**). **Tables 2** and **3** list model input variables for the concrete and steel fibers, respectively, in which the notations refer to those in **Fig. 2(b)**. Elastic beam-column elements are adopted to model the RC cap. The ERBs are modeled using a bilinear relationship (Zhang and Huo 2009), as illustrated in **Fig. 2(d)**, where G_b = 1200kN/m is the shear modulus of the rubber, t_r = 0.07 m is the total height of the rubber layers, and A_b is the total area of the ERBs determined following AASHTO (2012). Accordingly, other variables in **Fig. 2(d)** can be determined. This

ERB model is assigned to the horizonal degree-of-freedom while other degree-of-freedoms are fixed.

Table 2. Model input variables of the Concrete04 material for concrete

Component	$f_{c,cover}$ MPa	$\varepsilon_{c,cover}$ /	$\varepsilon_{cu,cover}$ /	$f_{c,core}$ MPa	$\varepsilon_{c,core}$ /	$\varepsilon_{cu,core}$ /
Column	34	0.002	0.005	40.58	0.0039	0.0147
Pile	34	0.002	0.005	39.20	0.0035	0.0132

Note: Variables refer to **Fig. 3(b)**.

Table 3. Model input variables of the Steel02 material for rebars

f_y MPa	E_s GPa	b /	R_0 /	CR_1 /	CR_2 /	a_1 /	a_2 /	a_3 /	a_4 /
400	200	0.01	20	0.925	0.15	0	1	0	1

Note: Steels in the column and piles share the same mechanical properties. R_0, CR_1 and CR_2 are variables to control the transition from elastic to plastic branches; a_1, a_2, a_3, and a_4 are isotropic hardening parameters. Other variables refer to **Fig. 3(c)**.

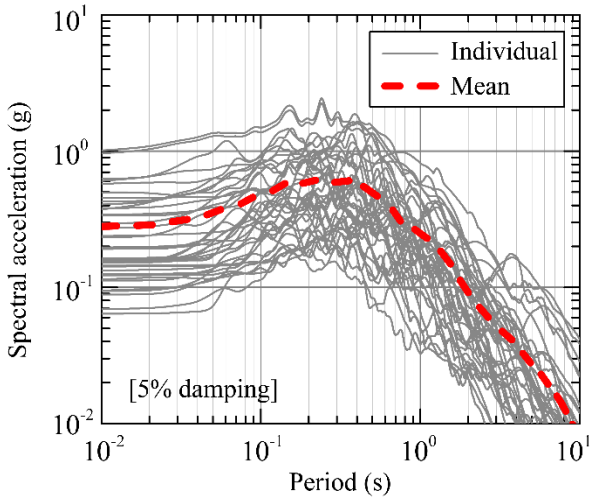

Fig. 4 Acceleration spectra of the adopted 40 ground motions

To produce reliable fragility curves, a large number of ground motions ought to be used to establish accurate PSDMs in advance. On the other hand, however, nonlinear dynamic analyses are often time-consuming. Therefore, from a view of practice, 40 real site unscaled ground motions are adopted for each case. **Fig. 4** shows acceleration spectra of these ground motions and their mean spectrum. The 40 ground motions are selected by Baker et al. (2011) for rock sites at California. It is worth noting that the embedded depths for piles are as large as 30 m, the bottom of which is supposed to stand on a quite firm soil layer on top of the bedrock. Recalling the abovementioned all fifteen cases considered, a total number of 40 × 15 = 600 dynamic analyses are run in this study.

Three engineering demand parameters (EDPs) are considered, including the bearing deformation, the peak column curvature and the peak pile curvature. For conciseness, this study merely considers their slight damage states. **Table 4** lists capacity values and their dispersions for the slight damage states. More specifically, the capacity value for bearing deformation refers to a 100% shear strain regarding the above defined 0.07 m height of the rubber layers. The

capacity values for column and pile curvatures represent the occurrence of first-rebar yielding.

Table 4. Capacity values and dispersions for EDPs at slight damage states

EDP	Unit	Capacity	Dispersion
Bearing deformation	m	0.07	0.25 [a]
Column curvature	1/m	1.714×10^{-3} †	0.59 [b]
Pile curvature	1/m	3.556×10^{-3} †	0.59 [b]

[a](Padgett et al. 2010);
[b](Nielson and DesRoches 2007);
†Capacity values for the base case with parameters having the mean values. These values may vary for cases with lower and upper bounds of the parameters.

RESULTS AND DISCUSSION

Before showing the sensitivity results, **Fig. 5** displays indicative results about the impact of scour depth on fragility curves for different EDPs for the base case. Note that $S_{a\text{-}20}$ (spectral acceleration at the period of 2.0 s) is adopted as the IM in this study based on the authors' recent study (Wang et al. 2018) on optimal IMs for PSDMs of bridges in liquefiable ground.

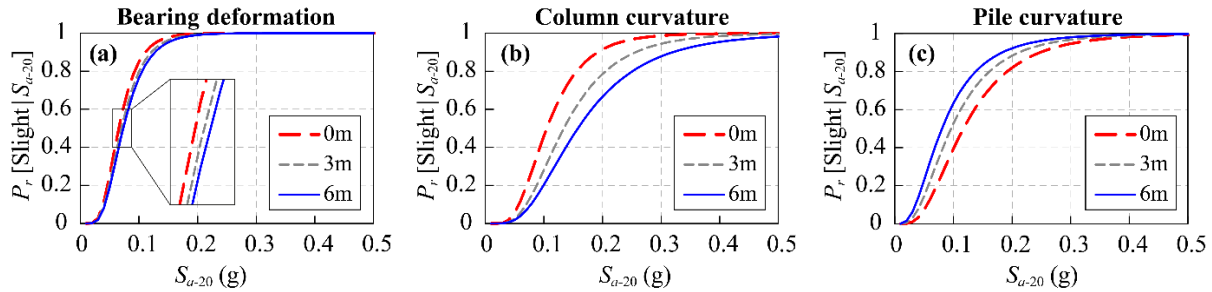

Fig. 5 Impact of scour depths on fragility curves for different EDPs for the base case: (a) bearing deformation, (b) column curvature and (b) pile curvature

From a quick inspection of **Fig. 5**, it is seen that the scour depth has a minor impact on the performance of the bearing, while it has significant impacts on that of the column and pile curvature. This result indicates that columns and piles are generally more sensitive components than bearings with respect to the scour depth. Specifically, the probabilities of exceedance (P_r) for the column curvature at the slight damage state decrease significantly with the increase of scour depth (**Fig. 5(b)**). This is partially attributed to the isolation effect induced by the increase of scour depth, which reduces the lateral constraint to the piles and in turn elongates the periods of bridges. By contrast, P_r for the pile curvature apparently increase with the increase of scour depth (**Fig. 5(c)**), which emphasizes the role of soil-pile interaction effect in the estimates of seismic performance of bridges under scour. Theoretically, scour has two-fold effects on the pile demands: (1) increasing the periods of bridges, which may generally reduce the demands; (2) increasing the lateral deflections of piles, which inevitably increases the resistances provided by the soils. The increased soil resistances in turn counteract the reduced demands due to the elongation of periods. Therefore, the final effect of scour on the fragility curves for pile curvature depends on which effect dominates. In general, it is seen that the increase of scour depth tends to transfer the damage mechanism of scoured bridges in liquefiable ground from columns to piles. This result is generally consistent with previous studies on a short and a medium span RC bridges, each with a specific configuration, in scoured and nonliquefiable ground (Wang et al. 2014). Nevertheless, it should be noted that the results in the present study

are based on the base case with mean-valued parameters. Whether they would change in other cases with different geometric configurations requires further assessments.

Figs. 6 to **8** display tornado diagram results for sensitivity-ranking of the studied parameters with respect to different EDPs of the bridges under different scour depths. For the seismic performance of bridges in terms of bearing deformation (**Fig. 6**), the axial compressive ratio of column (R_{ac}) and its height (H) tend to be the most sensitive parameters across all the scenarios (with and without scour). In particular, larger H and R_{ac} tend to reduce the P_r of bearing deformation at the slight damage state (i.e., blue bars are located at the right side of the Tornado diagram, recalling **Fig. 2** for more details). The less sensitive parameters for the scenario without scour (**Fig. 6(a)**) are the relative densities of sands ($D_{r\text{-}LS}$ and $D_{r\text{-}DS}$ at the third and fourth places, respectively). However, these two parameters show the least sensitivities for the scoured scenarios, especially for $D_{r\text{-}LS}$. This phenomenon is partially attributed to the decrease of loose sand layer thickness with the increase of scour depth, which in turn reduces the contribution of the loose sand layer to the performance of bridges. By contrast, the pile and column diameters (d and D) that show the least sensitivities in the scenario without scour become less sensitive for the scoured scenarios; i.e., they are just behind the most sensitive two parameters in the 3 m scoured scenario and further rise in the scenario with a scour depth of 6 m. This result implies that the column and pile diameters should be carefully designed for bridges under severe scour conditions.

For the performance of bridges in terms of column curvature (**Fig. 7**), H and D are the most sensitive parameters, regardless of with or without scour, as expected. Cases with smaller H and larger D tend to have relatively lower P_r. A generally similar tendency is observed for the relative densities of sands as compared to the abovementioned EDP of bearing deformation; that is with the increase of scour depth, they change from quite sensitive parameters to the least sensitive ones. In addition, pile-related parameters (d and S) show notable sensitivities in the scoured scenarios as compared to the scenario without scour. This phenomenon once again highlights the importance of the pile-related parameters in the seismic design of bridges under scour and liquefaction hazards. In addition, it is somewhat surprising to find that R_{ac} becomes the stably low sensitive parameter for the estimate of column performance in terms of curvature, which may be because that the variation in the column flexural demand due to the varied superstructure inertial force counteracts that in the flexural capacity of the column section.

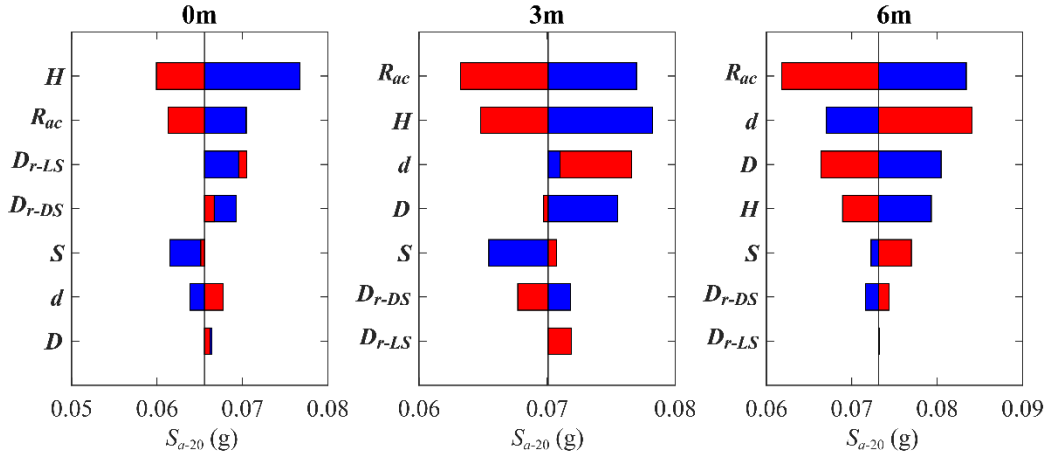

Fig. 6 Impact of scour depth (0 m, 3 m, 6 m) on Tornado diagram for bearing deformation

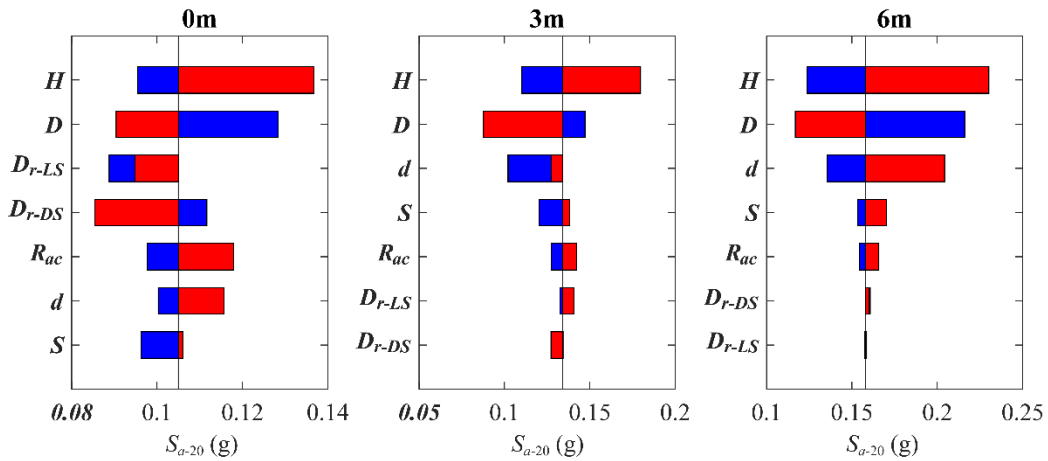

Fig. 7 Impact of scour depth (0 m, 3 m, 6 m) on Tornado diagram for column curvature

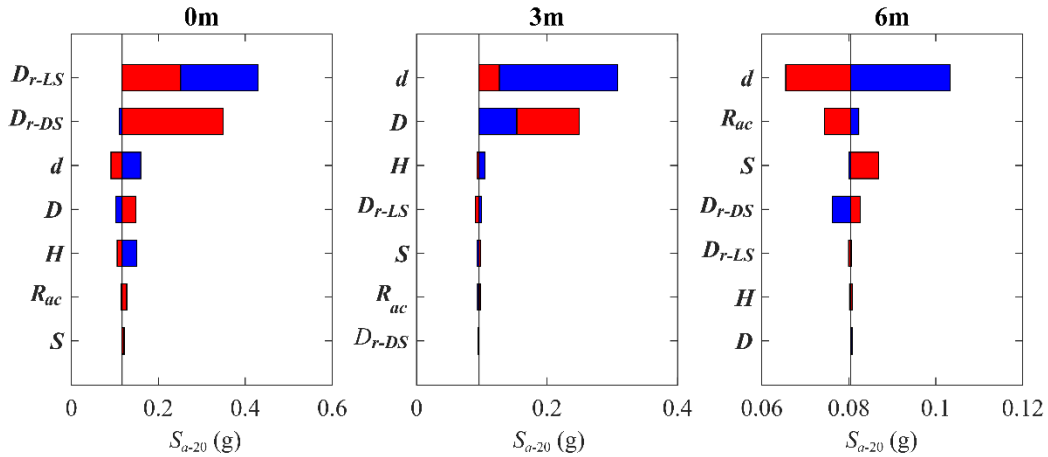

Fig. 8 Impact of scour depth (0 m, 3 m, 6 m) on Tornado diagram for pile curvature

As for the performance of bridges in terms of pile curvature (**Fig. 8**), the scour depth shows significant influences to the sensitivity-ranking of the parameters. $D_{r\text{-}LS}$ and $D_{r\text{-}DS}$ are the most sensitive parameters for the scenario without scour. Then, the sensitivity of $D_{r\text{-}LS}$ tends to decrease with the increase of sour depth, which should be owing to the decrease of loose sand layer thickness due to scour. As for $D_{r\text{-}DS}$, however, it displays almost zero sensitivity for the scenario with a scour depth of 3 m, but again shows visible sensitivity for the 6 m scoured scenario, which may be attributed to the large pile deflection-induced dense sand-pile interaction effect for this scenario (note that loose sand layer is relatively thin in this scenario, see **Fig. 3(a)**). By contrast, the pile-related parameters (*d* and *S*) generally exhibit increasing sensitivities with respect to the scour depth varied from 0 m to 3 m and 6 m, which twice again highlights the paramount role of piles in the seismic design of bridges under the combined effect of scour and liquefaction hazards. In addition, although the column-related parameters show different ranks of sensitivity with respect to the pile curvature, their sensitivities are mostly quite small.

SUMMARY AND CONCLUSIONS

This paper focuses on the sensitivity of seismic performance of bridges under combined effects of scour and liquefiable hazards. A fragility-based Tornado diagram method is proposed for the sensitivity analyses. Column-, pile- and soil-related seven primary parameters are studied,

which are assumed to follow normal distributions. The 16th and 84th percentiles of these parameters are selected as lower and upper bounds for the sensitivity analyses. Coupled soil-bridge finite element (FE) models are built to perform probabilistic seismic demand analyses (PSDA). Three scenarios with scour depths of 0 m (without scour), 3 m and 6 m (with scour) are studied. Monitored engineering demand parameters (EDPs) include the bearing deformation, column curvature and pile curvature. The PSDA results are further used to establish fragility curves for the FE models that represent variations of the studied parameters. Intensity measures at median fragility values (probability of exceedance equal to 50%) derived from the fragility curves are selected as performance indices to form the Tornado diagrams.

It is found that among the studied parameters, the axial compressive ratio of column (R_{ac}) and its height (H) are the most sensitive parameters for estimates of the bearing performance across all scenarios with and without scour. As for the performance of column, the column diameter (D) and H have the most significant effects regardless of with or without scour, followed by the pile diameter (d) and its center-to-center distance (S), which tend to show gently increasing sensitivities with the increase of scour depth. The scour depth shows significant effects on sensitivities of parameters for capturing the pile performance, where the pile-related parameters (d and S) generally exhibit notable influences for the scoured scenarios. Clearly, these two parameters should be carefully treated in the seismic design of bridges under combined effects of scour and liquefaction hazards. On the other hand, for all the studied EDPs, the relative densities of loose and dense sands ($D_{r\text{-}LS}$ and $D_{r\text{-}DS}$) have significant influences in the scenario without scour. However, they generally become the least sensitive parameters for scenarios with scour.

ACKNOWLEDGMENT

This work is supported by the National Nature Science Foundation of China (51778469) and the China Postdoctoral Science Foundation. Any opinions, findings, and conclusions expressed are those of the authors, and do not necessarily reflect those of the sponsoring organizations.

REFERENCES

AASHTO. (2012). *AASHTO LRFD bridge design specifications*. American Association of State Highway and Transportation Officials (AASHTO), Washington, D.C.

Baker, J., Lin, T., Shahi, S., and Jayaram, N. (2011). *New ground motion selection procedures and selected motions for the PEER transportation research program*. Pacific Earthquake Engineering Research Center, Berkeley, CA.

Bhattacharya, S., Tokimatsu, K., Goda, K., Sarkar, R., Shadlou, M., and Rouholamin, M. (2014). "Collapse of Showa bridge during 1964 Niigata earthquake: A quantitative reappraisal on the failure mechanisms." *Soil Dynamics and Earthquake Engineering*, 65, 55–71.

Brandenberg, S. J., Boulanger, R. W., Kutter, B., and Chang, D. (2005). "Behavior of pile foundations in laterally spreading ground during centrifuge tests." *Journal of Geotechnical and Geoenvironmental Engineering*, 131(11), 1378–1391.

Brandenberg, S., Kashighandi, P., Zhang, J., Huo, Y., and Zhao, M. (2008). "Sensitivity study of an Older-Vintage Bridge subjected to lateral spreading." *Geotechnical Earthquake Engineering and Soil Dynamics IV*, ASCE, Reston, VA.

Brandenberg, S., Kashighandi, P., Zhang, J., Huo, Y., and Zhao, M. (2011). "Fragility functions for bridges in liquefaction-induced lateral spreads." *Earthquake Spectra*, 27(3), 683–717.

Cornell, C. A., Jalayer, F., Hamburger, R., and Foutch, D. (2002). "Probabilistic basis for 2000

SAC federal emergency management agency steel moment frame guidelines." *Journal of Structural Engineering*, 128(4), 526–533.
Deng, L., Wang, W., and Yu, Y. (2016). "State-of-the-art review on the causes and mechanisms of bridge collapse." *Journal of Performance of Constructed Facilities*, 30(2), 04015005.
Jones, A., Kramer, S., and Arduino, P. (2002). *Estimation of uncertainty in geotechnical properties for performance-based earthquake engineering*. *PEER Report*, Pacific Earthquake Engineering Research Center, Berkeley, CA.
Klinga, J., and Alipour, A. (2015). "Assessment of structural integrity of bridges under extreme scour conditions." *Engineering Structures*, 82, 55–71.
McKenna, F. (2011). "OpenSees: A framework for earthquake engineering simulation." *Computing in Science and Engineering*, 13(4), 58–66.
Mokwa, R. (1999). "Investigation of the resistance of pile caps to lateral loading." Ph.D. dissertation, Virginia Tech, Blacksburg, VA.
Nielson, B. , and DesRoches, R. (2007). "Analytical seismic fragility curves for typical bridges in the central and southeastern United States." *Earthquake Spectra*, 23(3), 615–633.
Padgett, J., Ghosh, J., and Dueñas-Osorio, L. (2010). "Effects of liquefiable soil and bridge modelling parameters on the seismic reliability of critical structural components." *Structure and Infrastructure Engineering*, 9(1), 59–77.
Wang, S., Liu, K., Chen, C., and Chang, K. (2015). "Experimental investigation on seismic behavior of scoured bridge pier with pile foundation." *Earthquake Engineering and Structural Dynamics*, 44(6), 849–864.
Wang, X., Ye, A., and Luo, F. (2016a). "Sesimic response sensitivity analysis of pile supported bridge structures in liquefiable ground." *Gongcheng Lixue/Engineering Mechanics*. (in Chinese)
Wang, X., Luo, F., Su, Z., and Ye, A. (2017). "Efficient finite-element model for seismic response estimation of piles and soils in liquefied and laterally spreading ground considering shear localization." *International Journal of Geomechanics*, 17(6), 06016039.
Wang, X., Shafieezadeh, A., and Ye, A. (2018). "Optimal intensity measures for probabilistic seismic demand modeling of extended pile-shaft-supported bridges in liquefied and laterally spreading ground." *Bulletin of Earthquake Engineering*, 16(1), 229–257.
Wang, X., Ye, A., He, Z., and Shang, Y. (2016b). "Quasi-static cyclic testing of elevated RC pile-cap foundation for bridge structures." *Journal of Bridge Engineering*, 21(2), 04015042.
Wang, Z., Dueñas-Osorio, L., and Padgett, J. (2014). "Influence of scour effects on the seismic response of reinforced concrete bridges." *Engineering Structures*, 76, 202–214.
Zhang, J., and Huo, Y. (2009). "Evaluating effectiveness and optimum design of isolation devices for highway bridges using the fragility function method." *Engineering Structures*, 31(8), 1648–1660.